
Article:
Kantzas, E.P. orcid.org/0000-0002-7610-1874, Val Martin, M. orcid.org/0000-0001-9715-0504, Lomas, M.R. et al. (14 more authors) (2022) Substantial carbon drawdown potential from enhanced rock weathering in the United Kingdom. Nature Geoscience, 15 (5). pp. 382-389. ISSN 1752-0894

https://doi.org/10.1038/s41561-022-00925-2

Supplementary Information

Substantial carbon drawdown potential from enhanced rock weathering in the UK

Euripides Kantzas[1], Maria Val Martin[1], Mark R. Lomas[1], Rafael M. Eufrasio[2], Phil Renforth[3], Amy Lewis[1], Lyla L. Taylor[1], Jean-Francois Mecure[4,5], Hector Pollitt[5,6], Pim V. Vercoulen[5,6], Negar Vakilifard[7], Philip B. Holden[7], Neil R. Edwards[5,7], Lenny Koh[2], Nick F. Pidgeon[8], Steven A. Banwart[9,10] and David J. Beerling[1*]

[1]Leverhulme Centre for Climate Change Mitigation, Department of Animal and Plant Sciences, University of Sheffield, Sheffield S10 2TN, UK

[2]Advanced Resource Efficiency Centre, Management School, University of Sheffield, Sheffield S10 1FL, UK

[3]School of Engineering and Physical Sciences, Heriot-Watt University, Edinburgh Campus, Edinburgh EH14 4AS, UK

[4]Global Systems Institute, Department of Geography, University of Exeter, Exeter, UK

[5]Cambridge Centre for Energy, Environment and Natural Resource Governance, University of Cambridge, Cambridge, CB3 9EP, UK

[6]Cambridge Econometrics Ltd, Covent Garden, Cambridge CB1 2HT, UK

[7]Environment, Earth and Ecosystems, The Open University, Milton Keynes, MK7 6AA, UK

[8]Understanding Risk Research Group, School of Psychology, Cardiff University and the Leverhulme Centre for Climate Change Mitigation, Cardiff CF10 3AT, UK

[9]Global Food and Environment Institute, University of Leeds, Leeds LS2 9JT, UK

[10]School of Earth and Environment, University of Leeds, Leeds LS2 9JT, UK

*e-mail: d.j.beerling@sheffield.ac.uk

Contents

Supplementary Methods

1. Rock extraction scenarios

There are approximately 800 active mines in the UK that are responsible for the annual extraction and processing of 129 Mt/yr of rock aggregate. The British Geological Survey[1,2] distinguishes between 303 limestone/dolomite mines (76 Mt/yr), 264 sandstone mines (15 Mt/yr), and 228 igneous/metamorphic mines (38 Mt/yr).

Table S1 presents the breakdown of the 228 igneous/metamorphic mines by host rock type. 115 mines extract basic or ultrabasic rock types (basalt, gabbro or micro-gabbro, harzburgite, lamprophyre, tachylite)[1,2]. Assuming that the average size of production site is the same across all igneous rock types (~164 kt/yr), basic and ultrabasic rock production is approximately 19 Mt/yr.

The production of rock aggregate in the UK increased in the second half of the 20th century from 25 Mt/yr in 1945 peaking at 200 Mt/yr in 1990, and subsequently decreasing to present values[2,3]. Similarly, consumption of rock per capita in the UK has dropped from 3.5 t in 1990 to approximately 1.9 t. The annual 10-year rolling average of rock extraction shows maximum increases of 15.4% (1960's), which potentially constrains a feasible rate of capacity scale-up.

Based on this information, we propose three scenarios for future basic rock extraction in the UK.

Scenario 1: 'no additional extraction sites'. We assume that per capita production of aggregate will continue to fall from 1.9 to 1.5 t/yr by 2032 and remain constant thereafter. This represents a total rock demand of 106 Mt/yr by 2036 increasing to 110 Mt/yr by 2050. Assuming that the proportion of this rock demand met by igneous rock remains at historical values (~29%) and that basic igneous rock extraction represents 50% of this (19Mt/yr to 15 Mt/yr by 2035). We assume that the production capacity for each extraction site is 198 kt/yr (an average from 2006 and 2018, which are the only two years BGS report values), equating to ~96 sites. Scenario 1 assumes that the same number of extraction sites will remain operational, and that the spare capacity from a reduction in demand will be used for ERW. It also assumes that in 2025 the average production per site would increase to the 2006 value (225kt/yr), by 2035 this would increase further to 338 kt/yr, and that post 2050 this would increase to 450 kt/yr. It is not untypical for a mine to produce up to a Mt/yr of crushed rock, with 'super quarries' able to supply several Mt/yr. As such the expansion in capacity is plausible given that demand would increase from ERW, while the total number of sites is constrained. We also assume in this scenario and all others that 15% of the rock extracted would be classified as 'fines' which is also suitable for ERW.

Scenario 2: 'slow increase capped at 100Mt/yr'. As in S1, we assume that aggregate demand will continue to reduce, and that maintaining existing capacity would supply material for ERW. This is maintained until 2035, following this we assume a scale up in rock extraction of 7% (half the historical maximum) until total additional capacity is 100 Mt/yr (in 2057). The total rock extracted (aggregate + ERW) in the UK under this scenario would be equivalent to the maximum historical value in 1990.

Scenario 3: 'fast increase capped at 160 Mt/yr'. This would follow S2 until 2035, following this we assume a scale up in rock extraction of 15% (slightly less than the historical annual 10-year rolling average of 15.4%) until total additional capacity is 160 Mt/yr (in 2049). The total rock extracted in the UK under this scenario would be unprecedented, representing a 40% increase over the 1990 maximum.

The total number of new mines would depend on their size. If these were similar to the current average (~250 kt/yr) it would require opening approximately 10 per year between 2035 and 2050 for S2 and S3. However, if production were concentrated in larger sites (~1 Mt/yr), between approximately 3 (S2) and 7 (S3) new mines would be required per year between 2035 and 2050.

2. UK basalt mineralogy

All simulations were undertaken for three UK basalts (Cragmill, Middleton and Hillhouse) sourced from commercial quarries (Breedon Group) with specified mineralogies (Table S2) determined using X-ray Diffraction (XRD). Cragmill[4] and Middleton are mined from the Carboniferous (Pennsylvanian) Whin Sill (dolerite) emplacement (Cragmill Quarry, Belford, Northumberland, NE70 7EZ; Middleton, Forcegarth Quarry, Durham, DL12 0EP) and Hillhouse[4] from a Carboniferous intrusive gabbro (Hillhouse Group, Hillhouse Quarry, Troon, Ayrshire, KA10 7HX). Mineralogy data for Cragmill and Hillhouse are reported in Ref (4). The mineralogy data for Middleton were newly measured for this study using the same XRD methods, instruments and interpretation software as described previously[4]. For modelling purposes, we adopted standardised mineralogies across all basalts, as defined in Table S2.

3. Drivers

Top-soil pH was obtained by spatially averaging two high resolution gridded datasets (1 × 1 km, 0.05° × 0.05°, respectively)[5,6] with resulting pH distribution over croplands similar to measurements of over 200,000 agricultural soil samples[7]. High resolution monthly soil temperature and precipitation data (0.1°x0.1°) from a global, multi-model data assimilation system[8] provide a baseline UK current climate (2001-2015) on which monthly anomalies of soil temperature and precipitation (2020-2070) from CLM5 were superimposed.

We used a high-resolution vector crop cover map (scale: 1:2500, minimum unit: 2 ha) for the UK[9] with 8 crop classes: spring/winter wheat, spring/winter barley, field beans, maize, oilseed rape, and potatoes. This assumes stationarity in the current geographies of arable cropping across the scenarios. CLM5 includes parametrizations for spring wheat and maize, and we obtained monthly fields of net primary production (NPP), evapotranspiration, soil respiration, soil field capacity and irrigation for 2020-2070. These outputs were spatially interpolated to match the resolution of the crop cover map and overlaid to get monthly fields of spring wheat and maize on the appropriate locations. To compute NPP for the other crop types represented by the crop cover map, we obtained annual UK yields for each crop[9] for the period 2000-2019 and converted them to NPP after ref.[10]. Using this data, we build linear regression models to obtain a relationship between annual NPP of spring wheat and each of the remaining crops (p <0.05 for all crops except field beans), thus obtaining annual NPP for each crop type in each grid-cell by using CLM5 simulated values of spring NPP as a predictor variable. The monthly distribution of NPP for each crop was obtained by normalizing the monthly time series of spring wheat NPP from CLM5 in each grid-cell, to sum to the desire annual NPP for each crop as obtained from its regression model and then shifting the signal according to UK-specific crop calendars, using a delay signal function.

Using CLM5 spring wheat monthly data, we employed regression trees[11] to build a predictive model with monthly transpiration as a target variable and monthly air temperature and NPP as predictor variables (R^2 = 0.92, 5-fold cross-validation). We then drove this model with the NPP of the remaining crops to calculate corresponding transpiration for their respective grid cells. A similar approach was used for evaporation (R^2 = 0.69). For soil respiration, the predictor variables were NPP, soil temperature and soil field capacity (R^2 = 0.72). All datasets were re-gridded to 1/24° resolution by spatial interpolation.

4. ERW model sensitivity to environmental and biological drivers

For these analyses, we report first year of the simulations presented in the main manuscript, with a focus on two sites having high and low weathering rates for the Cragmill basalt ($p80$ = 100 μm). In these tests, each driver varies, with the other drivers held constant. Carbon Dioxide Removal (CDR) is defined as the sum of removal pathway 1 (soil carbonate formation/dissolution) and pathway 2 (alkalinity production). Pathway 2 leads to ocean CDR, calculated here with an empirical function accounting for ocean PCO_2, ocean temperature and salinity[12,13].

4.1. Response to soil pH. Modelled weathering and hence CDR is particularly sensitive to soil porewater pH (Figure S1a) and displays pH-dependent behaviour expected when weathering the constituent silicate minerals found in basalts[14,15]. CDR is almost twice as large at pH~4 as at circumneutral pH, but begins to rise slightly above pH~8 due to the hydroxyl-promoted dissolution of key tectosilicate and inosilicate minerals (Table S3). The difference between the results for the two sites shown in Figure S1a is largely explained by their different soil pH values. The majority of UK cropland sites (green shading, Figure S1a), pH (5.6–7.4) are slightly acidic to circumneutral with greater CDR at more acidic conditions where silicate rock weathers more rapidly; CDR drops by one third across this range.

4.2. Soil temperature. Weathering rates increase as temperature increases following mineral-specific Arrhenius functions, and therefore modelled CDR increases by a factor of ~1.4 as mean annual temperature rises from 2°C to 12°C for both a low pH (fast weathering) and higher pH (slower weathering) site (Figure S1b). Over the UK temperature range of 7.3–9.8°C (green shading), CDR increases by a factor of ~1.1 (~10%) as temperature rises.

4.3. Crop net primary productivity (NPP). NPP has a comparatively modest effect on total CDR via effects on weathering, being <0.2 tCO_2 ha^{-1} y^{-1} or 9–12% as NPP rises from 400 to 1200 gC m^{-2} yr^{-1} (Figure S1c). Over UK croplands, the NPP range (365–891 gC m^{-2} y^{-1}, green shading), leads to CDR increases by a factor of ~1.1 (~10%). This effect arises from two separate aspects of the enhanced rock weathering (ERW) model: soil acidification due to harvest (Section 2.3.1) and the overall effect of rhizosphere processes (Section 2.3.2).

4.3.1. Harvest effects as a function of NPP. Harvest results in removal of nutrients from the system, which is quantified from NPP using the CLM5[16] harvest index (0.85). Senescing biomass would otherwise return nitrogen in the form of ammonium, phosphorus, base cations and sulphate to the soil, resulting in net input of alkalinity. This loss of nutrients from the soil system is a well-known cause of long-term soil acidification[17]. We account for this with an empirical alkalinity correction based on observations; given average nitrogen, HPO_4^{2-}, base cation and sulphur concentration[18], the alkalinity lost to the system is 0.0395 Eq mol^{-1} C harvested. We neglect micronutrient (e.g., Fe and Mn) effects in this analysis.

4.3.2. Rhizosphere processes as a function of NPP. Rhizosphere processes linked to plant productivity affect rhizosphere chemistry and weathering rates, including nutrient uptake from solution, uptake by mycorrhizal fungi and rhizosphere bacteria in direct contact with minerals, and chelation of mineral surfaces by organic anions exuded by roots, fungi and microbes. These processes are not explicitly represented in the ERW model, but are instead accounted for with an empirical function for capturing their net effect on weathering rates based on observations[13].

Within CLM5, acquisition of ammonium and nitrate by roots, and mycorrhizal fungi, along with nitrogen fixation, are calculated for plant functional types by the Fixation and Uptake of Nitrogen (FUN) model as a function of crop requirements[19]. The crop uptake demand for N satisfies stoichiometric relationships between biomass carbon and nitrogen, and represents total uptake whether from solution or via intimate fungal contact with decomposing biomass. Both

nitrate and ammonium are taken up from solution by plants and mycorrhizal fungi in competition with soil microbes in CLM5, but uptake of other nutrients sourced from minerals and possible organic acid exudates which may enhance weathering are not explicitly represented.

In our current model framework, total nitrate and ammonium uptake by both microbes and plants plus mycorrhizal fungi are included in the acidity balance derived for the CLM5 nitrogen cycle (Table S3). Comparing the net acidity due to ammonium and nitrate uptake with the total acidity from all components of the nitrogen cycle (Table S2, S3 and Section 3) suggests that CLM5 nitrogen uptake by crops and their mycorrhizal symbionts has a minor effect on soil solution acidity. It therefore comprises a negligible fraction of total rhizosphere effects on weathering.

4.4. Water flow through the soil profile. Vertical flow rate of water in the model soil column is directly proportional to precipitation–evapotranspiration from CLM5, with the proviso of no flow when volumetric water content is below field capacity. Because of chemical affinity[20,21], weathering rates slow as the porewaters become saturated by weathering products (concentration C as dissolved equivalents of each mineral) with respect to each mineral solubility equilibrium (Ceq). Therefore rates are expected to increase with greater flushing. These effects are accounted by calibrating our model for a chemical affinity term ($1–C/C_{eq}$) that is determined for each mineral and multiplied with the associated irreversible mineral dissolution rate[13]. Soil water content is adjusted according to monthly flow, which can be negative when evapotranspiration exceeds precipitation. Modelled CDR is less sensitive to model flow rate than to pH or temperature, increasing by a factor of less than 1.2 over the UK cropland range of flow rates (461–849 mm y^{-1} for 90% of sites), and it is site specific (Figure S1d). Similar general trends of increased CO_2 consumption with both increased temperature and increased flow rate have been observed for regional-scale weathering of basalt bedrock worldwide[22].

5. ERW model sensitivity to nitrogen fertilisers

We conducted two five-year land surface model (CLM5) sensitivity runs (2000–2004) to explore the effects of the nitrogen fertilisers on ERW and CDR; case 1 where nitrogen fertilisers are eliminated (0×Nfert) and case 2 where nitrogen fertilizer application rate is doubled (2×Nfert) with respect to the standard fertilisation scheme[16]. In these runs, fertiliser application rates varied across the UK from 0 kt N yr^{-1} to ~1200 kt N yr^{-1}. In CLM5, manure is applied at a constant rate of 0.002 kg N m^{-2} yr^{-1}. Ammonium fertiliser application commences at leaf emergences and continues for 20 days; rates vary with crop, time and location[16]. CLM5 does not apply nitrate fertilisers; all applied N goes to the ammonium pool. CLM5 fertiliser effects are therefore expected to be greatest in springtime, and to increase weathering rates by adding acidity and decreasing soil solution pH.

5.1 Net acidity generated by the CLM5 nitrogen cycle. The effect of the nitrogen cycle on the soil acidity balance (Extended Data Figure 3) is derived from the reactions in Table S4, whereby each nitrogen transformation is associated with the production or consumption of hydrogen ions. We assigned a stoichiometric acidity flux $\Delta H_{i,N}$ (mol H^+ mol^{-1} N) to each nitrogen flux $F_{i,N}$ (gN m^{-3}soil s^{-1}) calculated by the CLM5 code (Table S5). The product ($F_{i,N} \cdot \Delta H_{i,N}$), with appropriate unit conversions, gives the acidity flux during the time-step Δt (s $month^{-1}$) for the i^{th} reaction of the CLM5 nitrogen cycle. Their sum (Eq S1) is therefore the total change in acidity $\Delta Acidity_N$ due to the CLM5 nitrogen cycle:

$$\Delta Acidity_N = \sum(F_{i,N} \cdot \Delta H_{i,N}) / 14.0067\, \Delta t \qquad \text{(Eq S1)}$$

where 14.0067 gN mol^{-1} N is the atomic weight of nitrogen and the time-step is one month. Along with the Ca, Mg, K, and Na ions released from weathering the applied minerals, $\Delta Acidity_N$ contributes a negative term to the soil water alkalinity balance

$$Alk_t = Alk_{t-1} + 2\cdot (Ca_{weath}+Mg_{weath})+K_{weath}+Na_{weath} - \Delta Acidity_N \qquad \text{(Eq S2)}$$

used to calculate the soil pH[13].

For UK cropland sites over the three years (2002–2004), nitrogen fertilisers are the dominant contribution to $\Delta Acidity_N$ in the CLM5 topsoil (uppermost 20 cm) after they are applied each year. The fertiliser applications results in a peak in monthly $\Delta Acidity_N$ that is 10-fold higher during spring in the 2×Nfert case (Figure S2b) than that of the 0×Nfert case (Figure S2a), where the lower peak occurs much later during summer.

These effects are illustrated by depth for an example site (Figure S3) using the 0×Nfert and 2×Nfert simulations. Curves for the top 15 cm of soil during the 2002 growing season generated by the weathering model suggest that $\Delta Acidity_N$ is primarily important during the growing season as expected, with pH at least half a pH unit lower at 5 cm depth for the 2×Nfert case in June. At this site, the springtime $\Delta Acidity_N$ peak for the 2×Nfert case is amplified as the fertiliser signal propagates downward to this depth from May to June.

Pore water chemistry is calculated by depth over the top 15 cm of soil, where the acidifying contribution of N fertiliser appears in the spring and propagates downward, where the contribution of $\Delta Acidity_N$ to the total alkalinity is still observable below 15 cm in August, with a pH value that is a unit lower at 15cm for the 2×Nfert case (Figure S3). Otherwise, total alkalinity and pH differences between the 0×Nfert and 2×Nfert cases are modest in the subsoil.

These results suggest a modest net effect of nitrogen cycling on CDR (Figure S4). Over five years, CDR for the same site is slightly higher for the 2×Nfert case than for the 0×Nfert case. The net increase in cumulative CDR is ~0.1 tCO_2 ha^{-1} y^{-1} during the growing season and totals 0.4 tCO_2 ha^{-1} over five years. During the growing season, net CDR drops during spring into summer as the fertiliser acidity peak propagates downward through the soil profile, resulting in lower pH and less capture of pore gas CO_2. Net CDR rebounds as the acidity is discharged by flow in the autumn, with an increase in soil pH as vertical flow transports through the full soil profile the alkalinity that is produced by basalt weathering in the upper soil layers.

5.2 Net acidity generated during nitrogen uptake. The net acidity due to plant and mycorrhizal nitrogen uptake (Table S5) is defined as:

$$\Delta Acidity_{Nup} = F_{SMINN\_TO\_PLANT\_FUN\_NH4} - F_{SMINN\_TO\_PLANT\_FUN\_NO3} \qquad \text{(Eq S3)}$$

Figure S2 suggests that $\Delta Acidity_{Nup}$ is a minor component of $\Delta Acidity_N$ during the growing season when the nitrogen cycle has its greatest impact on weathering. During the growing season, the acidity contribution from microbial uptake (immobilisation) (Tables S4, S5, Figure S2), defined as:

$$\Delta Acidity_{Nimmob} = F_{ACTUAL\_IMMOB\_NH4} - F_{ACTUAL\_IMMOB\_NO3} \qquad \text{(Eq S4)}$$

is even smaller.

The fractions of total rhizosphere effects accounted for by $\Delta Acidity_{Nup}$ and $\Delta Acidity_{Nimmob}$ are minimal (S2). This indicates that utilizing the empirical NPP weathering-enhancement function[2] alongside the CLM5 nitrogen cycle is justified in accounting for the range of NPP and harvest effects on mineral dissolution.

6. Energy and economic modelling

We used an integrated energy-economy-carbon-cycle-climate model (Energy-Environment-Economy Macroeconometric-Future Technology Transformations-Grid Enabled Integrated Earth; E3ME)[23-25] to simulate the world enacting policies to limit global average temperature increase to 1.5°C (without overshoot). It is an updated version of the scenario used in Ref[26]. Policies included in the simulation include energy efficiency measures, carbon pricing and measures to promote the adoption of zero-carbon technologies in the power sector, personal transport and buildings. These policies are phased in from 2020 onwards and have been adjusted so that they are consistent with UK's net-zero and global 1.5°C temperature targets. Most of the policies in the simulation have already been implemented somewhere, but in the modelled scenario it is assumed that they are implemented in all nations. In the model simulation, global greenhouse gas emissions reach net-zero shortly after 2050. By 2050, the power sector has almost completely decarbonised and uses some bioenergy with carbon capture and storage, which compensates remaining emissions from industrial processes and agriculture. All other sectors have decarbonised mainly through electrification.

E3ME simulated UK energy and economic drivers (2020–2070) used in our ERW study are consistent with government policy[26]. The modelled evolution of UK energy supply and mix is consistent with specific policies in the 1.5°C scenario[26]. Median wage rates are determined by a set of econometric equations that are estimated and solved at sectoral level; wages increase in-line with economic growth rates. Industrial electricity tariffs are modelled with the rapid transition to renewable generation. Government support for the development of CCS also keeps generation costs down. Longer term continued learning effects reduce the costs of wind, solar and batter technologies, reducing overall generation costs. Diesel fuel prices remain largely unchanged in the long run. These results reflect the timing of the roll-out of electric vehicles in China, Europe and the US, which puts downward pressure on global oil prices. However, the remaining use of oil (e.g. for aviation or petrochemicals) means that low-cost sources are gradually depleted and oil prices recover (in real terms) in the longer term.

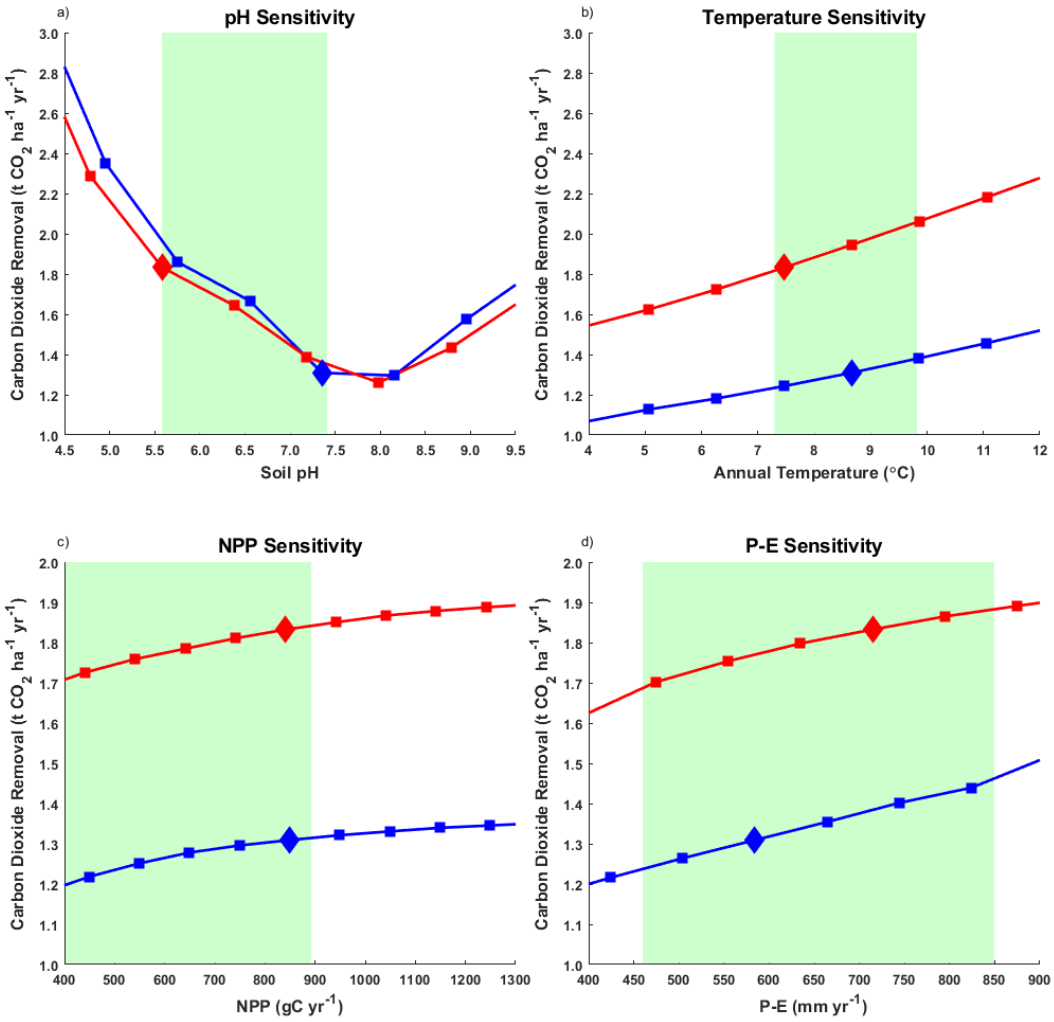

Figure S1. 1-D soil profile ERW model sensitivity to environmental and biological drivers. Curves represent illustrative sites with high (red curves) and low (blue curves) weathering rates of the Cragmill basalt ($p80$ = 100 µm). (**a**) Sensitivity to soil solution pH, (**b**) sensitivity to mean annual temperature, (**c**) sensitivity to crop net primary productivity (NPP) and (**d**) sensitivity to flow rate of water through the soil column (precipitation, P, minus evapotranspiration, E). Green shading denotes the range of 90% of cropland sites in the UK with respect to the X axis.

a)

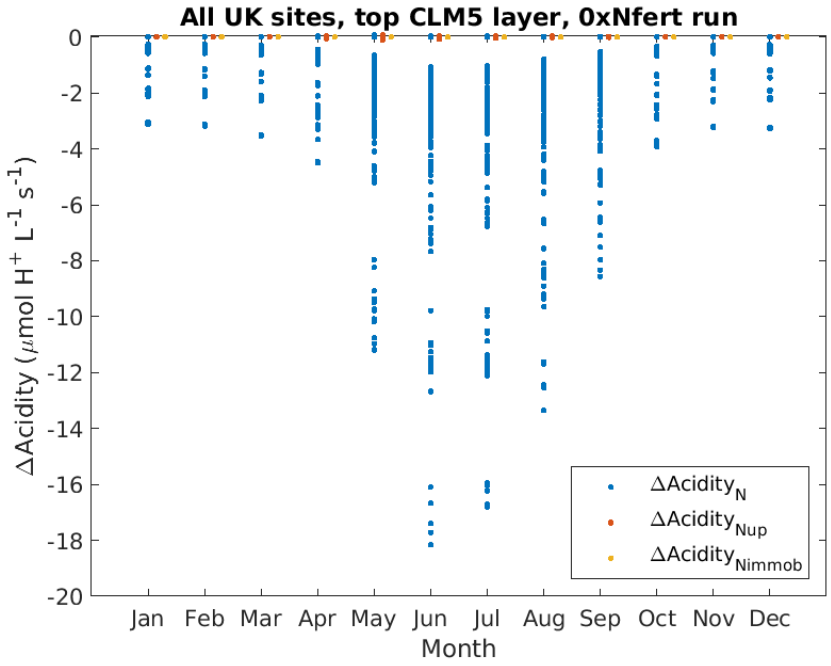

b)

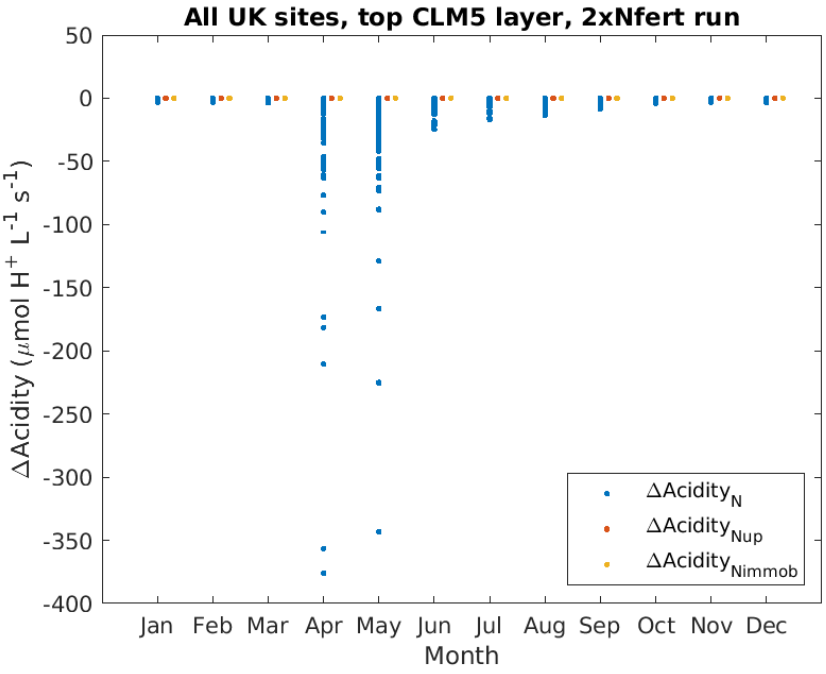

Figure S2. Monthly net acidity from nitrogen cycling in the CLM5 topsoil for (**a**) all UK sites and (**b**) sites with acidity exceeding 1 µmol H^+ L^{-1} s^{-1}. $\Delta Acidity_N$ is the total net acidity from the CLM5 nitrogen cycle (Eq. S1), $\Delta Acidity_{Nup}$ is the net acidity due to plant and mycorrhizal ammonium and nitrate uptake (Eq. S3), and $\Delta Acidity_{Nimmob}$ is the net acidity due to microbial ammonium and nitrate immobilisation (Eq. S4).

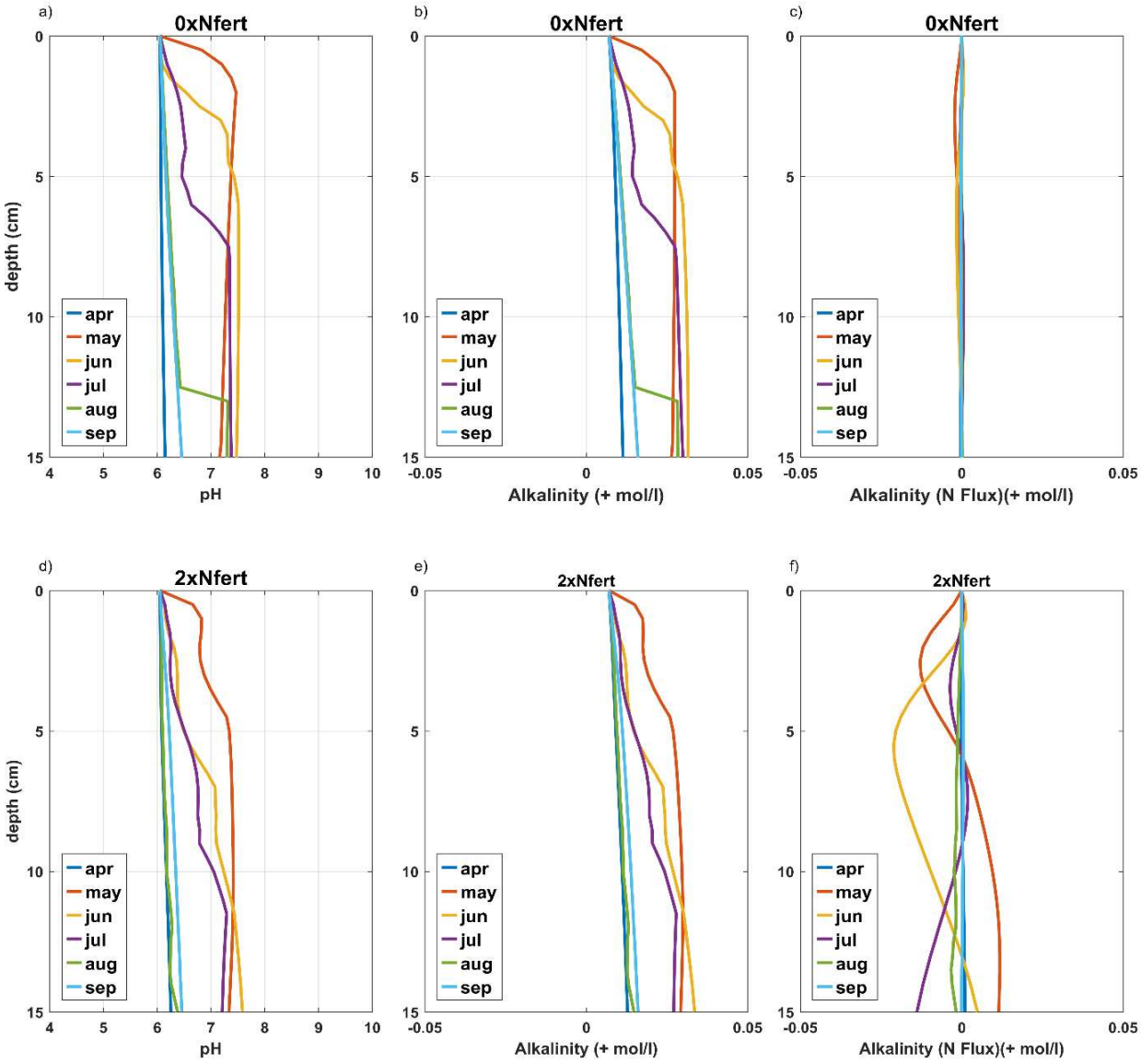

Figure S3. Depth-resolved soil acidity during the growing season at one site with medium weathering rates. (**a**) 0×Nfert case, soil column pH, (**b**) 0×Nfert total alkalinity, (**c**) 0xNfert case, alkalinity contribution from the CLM5 nitrogen cycle, (**d**) 2×Nfert case, soil column pH, (**e**) 2×Nfert case, total alkalinity, (**f**) 2×Nfert case, alkalinity contribution from the CLM5 nitrogen cycle.

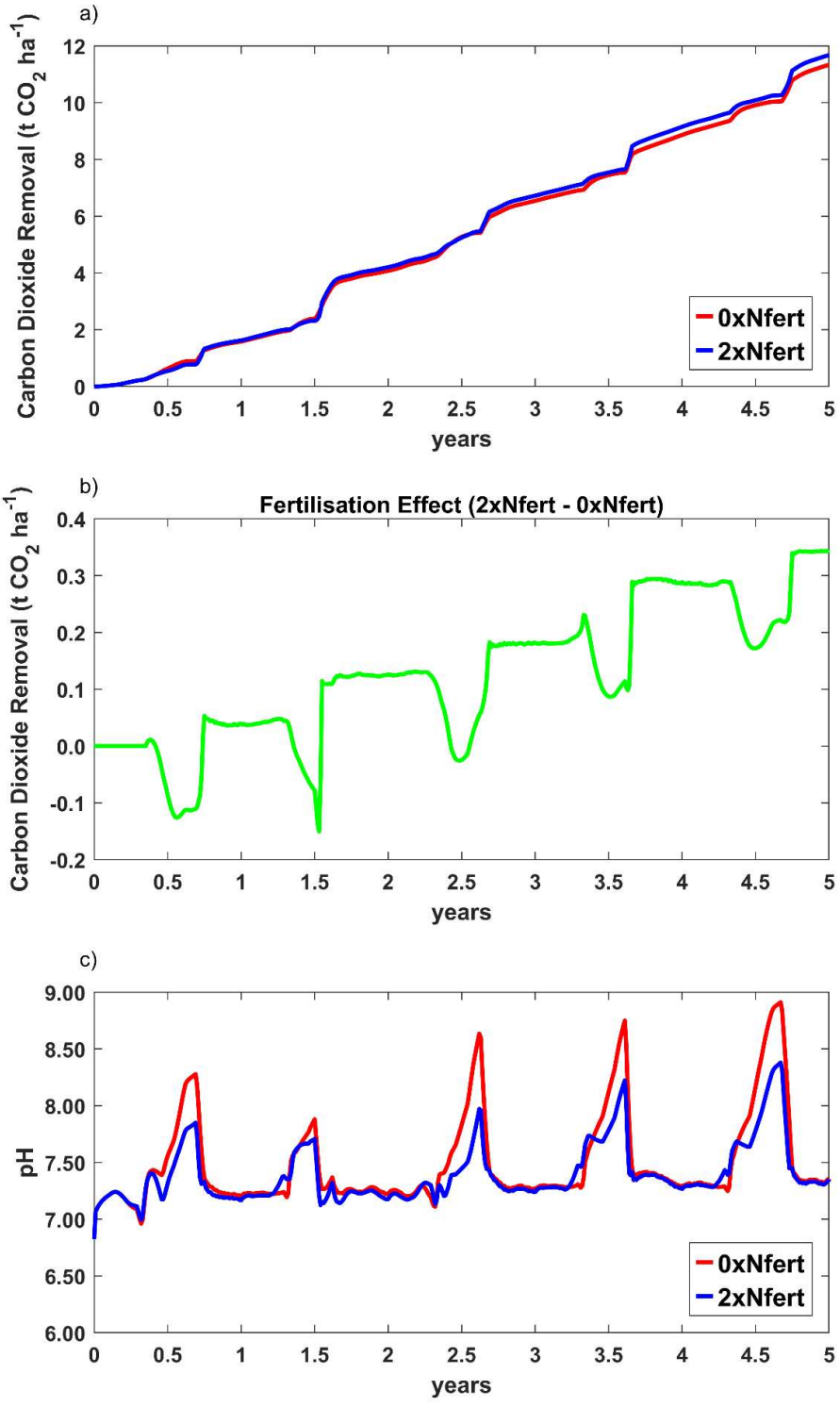

Figure S4. Changes in CDR due to CLM5 nitrogen cycling at one example site. This is the same site as shown in Figure S3. (**a**) cumulative CDR for the 0xNfert and 2xNfert cases. (**b**) CDR difference between 2×Nfert and 0×Nfert cases. (**c**) Mean soil column pH for the 0×Nfert and 2×Nfert cases.

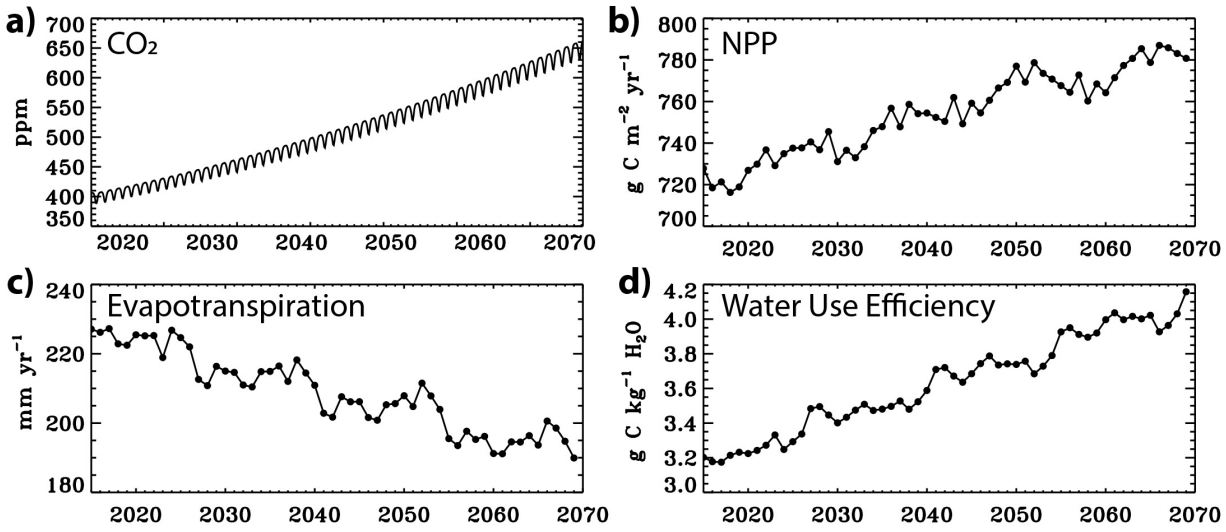

Figure S5. Trends in atmospheric CO_2, and simulated annual NPP, evapotranspiration and water-use efficiency. (a) Atmospheric CO_2 increased by ~200 ppm from 2015 to 2070, as defined in SSP3-7.0. In our CLM5 simulations with rising CO_2 and climate change, wheat (a dominant UK C_3 crop) NPP increased by 8% (b), evapotranspiration (Et) decreased by 21% (c) and water use efficiency (WUE, defined as NPP/Et) by 25% (d) between 2015 and 2070. Increasing NPP, and decreasing Et, facilitate weathering in our soil profile ERW model; increased NPP generates additional acidity stoichiometrically and decreased Et potentially increases the vertical soil water flux, defined as precipitation minus evapo-transpiration (plus irrigation), depending on climate (e.g., Fig. S1).

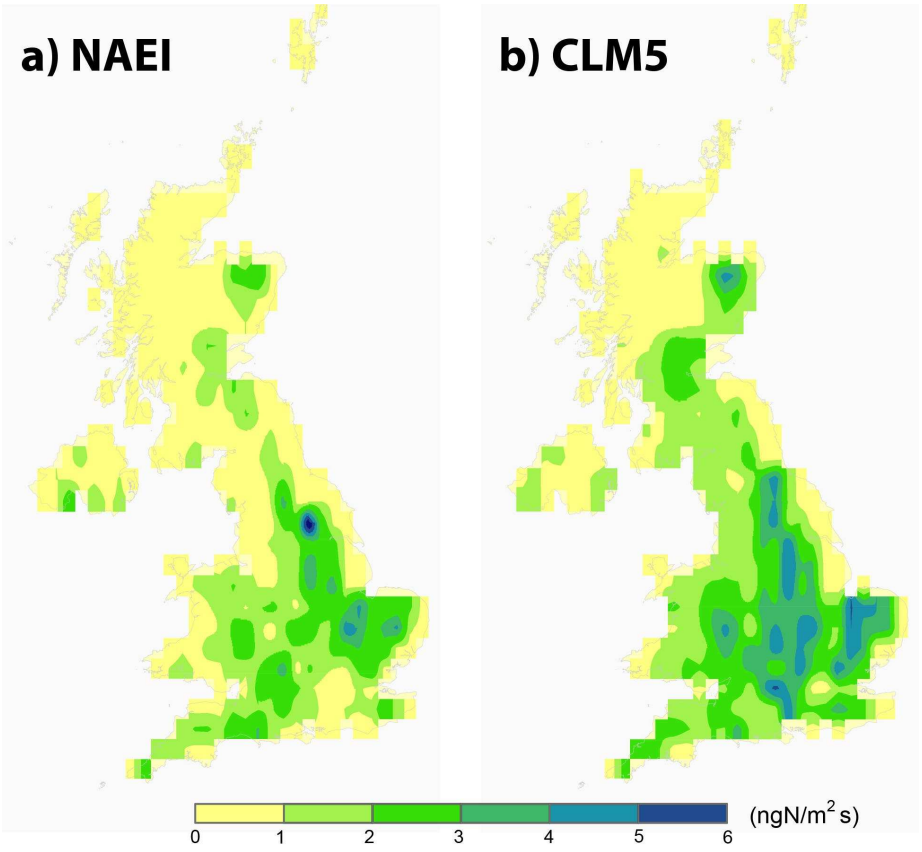

Figure S6. Spatial patterns of cropland soil N_2O fluxes. Annual averaged N_2O emissions from croplands (2016–2018) for (a) the UK National Atmospheric Emission Inventory (NAEI)[28] and (b) CLM5. To facilitate the comparison, NAEI N_2O emissions have been re-gridded from 1 × 1 km to the CLM5 resolution (23 ×31 km) and scaled using the gridded CLM5 crop fraction to represent emissions from synthetic fertilizer and manure on arable land. Spatial comparison of annual total N_2O emissions from arable croplands by CLM5 against NAEI on a grid cell-by-grid cell model-inventory was made by computing the Pearson's correlation coefficient (R) and the normalized mean bias (NMB; $\Sigma(Mi - Oi)/\Sigma(Oi)$, where Mi and Oi are simulated and inventory N_2O in each grid cell). CLM5 reproduces the spatial distribution of N_2O in the different regions across the UK, with a fairly good correlation against the UK-NAEI (R = 0.6), but with estimates slightly higher than the UK-NAEI (NMB = 5.1).

Table S1. UK mine distribution by rock type.

Type	SiO_2	Count
Andesite	57–63	8
Basalt	45–52	70
Clastic	-	9
Dacite	63–68	1
Diorite	57–63	18
Felsite	>65	5
Gabbro	45–52	41
Gneiss	>60	9
Granite	>70	25
Harzburgite	<45	1
Lamprophyre	<45	2
Melange	-	1
Pelite	>70	4
Psammite		20
Quartzite	>70	1
Rhyolite	69–77	1
Schist	-	2
Tachylite	45–52	1
Tonalite	>69	1
Trachyte	60–65	2
Tuff	-	4
Unidentified	-	2

Table S2. Mineral composition, weight fractions and chemical formulae of UK basalts considered in this study.

Basalt	Mineral	Percentage	Formula	Molecular weight
Cragmill[a]	Plagioclase	51.0%	$Ca_{0.6}Na_{0.4}Al_{1.6}Si_{2.4}O_8$	271.81
	Sanidine	9.1%	$Na_{0.35}K_{0.65}Al_{0.98}Si_{3.02}O_8$	274.3
	Augite	20.1%	$Ca_{0.9}Mg_{0.9}Na_{0.1}Al_{0.4}Fe_{0.2}Si_{1.9}O_6$	236.35
	Cordierite	3.3%	$Mg_2Al_4Si_5O_{18}$	584.95
	Quartz	8.4%	SiO_2	60.08
	Ilmenite	1.6%	$FeTiO_3$	151.73
	Phlogopite	0.8%	$KMg_3AlSi_3O_{10}(OH)_2$	417.27
	Chlorite-Smectite	3.4%	$Mg_{3.75}Fe_{1.25}Si_3Al_2O_{10}(OH)_8$	595.22
	Kaolinite	1.7%	$Al_2Si_2O_5(OH)_4$	258.16
	Apatite	0.8%	$Ca_5(PO_4)_3OH$	509.12
	Total	**99.96%**		
Middleton	Plagioclase	53.60%	$Ca_{0.6}Na_{0.4}Al_{1.6}Si_{2.4}O_8$	271.81
	Sanidine	5.50%	$Na_{0.35}K_{0.65}Al_{0.98}Si_{3.02}O_8$	274.3
	Augite	17.2%	$Ca_{0.9}Mg_{0.9}Na_{0.1}Al_{0.4}Fe_{0.2}Si_{1.9}O_6$	236.35
	Cordierite	1.3%	$Mg_2Al_4Si_5O_{18}$	584.95
	Quartz	6.5%	SiO_2	60.08
	Ilmenite	2.4%	$FeTiO_3$	151.73
	Phlogopite	3.8%	$KMg_3AlSi_3O_{10}(OH)_2$	417.27
	Chlorite-Smectite	8.6%	$Mg_{3.75}Fe_{1.25}Si_3Al_2O_{10}(OH)_8$	595.22
	Apatite	1.1%	$Ca_5(PO_4)_3OH$	509.12
	Total	**100.0%**		
Hillhouse	Plagioclase	34.6%	$Ca_{0.6}Na_{0.4}Al_{1.6}Si_{2.4}O_8$	271.81
	Augite	32.7%	$Ca_{0.9}Mg_{0.9}Na_{0.1}Al_{0.4}Fe_{0.2}Si_{1.9}O_6$	236.35
	Forsterite	14.7%	Mg_2SiO_4	140.71
	Spinel	4.5%	$MgAl_2O_4$	142.27
	Ilmenite	0.6%	$FeTiO_3$	151.73
	Analcime	7.1%	$NaAlSi_2O_6{\cdot}H_2O$	220.15
	Biotite	0.4%	$KMg_{2.5}Fe_{0.5}AlSi3O_{10}(OH)_2$	433.03
	Chlorite-Smectite	5.2%	$Mg_{3.75}Fe_{1.25}Si_3Al_2O_{10}(OH)_8$	595.22
	Apatite	0.1%	$Ca_5(PO_4)_3OH$	509.12
	Calcite	0.2%	$CaCO_3$	100.09
	Total	**99.98%**		

[a]Negligible calcite assessed from this XRD analysis of the Cragmill basalt.

Table S3. Kinetic parameters[4] of basaltic minerals: k is the log of the effective rate constant (mol m^{-2} s^{-1}), E_{app} is the apparent activation energy (kJ mol^{-1}), *n* is the reaction order of the weathering agents H^+ or OH^-, corresponding to acid, neutral and base kinetic parameters.

Mineral name	Min Prop. %	Acid			Neutral		Base		
		log10(*k*)	Eapp	*n*	log10(*k*)	Eapp	log10(k)	Eapp	*n*
Cragmill									
Labradorite	51.0	-7.87	42.1	0.626	-10.91	45.2	0	0	0
Sanidine	9.1	-10.06	51.7	0.5	-12.41	38	-21.2	94.1	-0.823
Augite	20.1	-6.82	78	0.7	-11.97	78	0	0	0
Cordierite	3.3	-3.8	113.3	1	-11.2	28.3	0	0	0
Quartz	8.4	0	-0	0	-13.99	87.7	-16.29	108366	-0.5
Ilmenite	1.6	-8.35	37.9	0.421	-11.16	37.9	0	0	0
Phlogopite	0.8	0	0	0	-12.4	29	0	0	0
Chlorite-smectite	3.4	-11.11	88	0.5	-12.52	88	0	0	0
Kaolinite	1.7	0.77	-13.18	22.2	-17.05	17.9	-0.47	-11.31	65.9
Apatite	0.8	-3.73	250	0.613	-8	250	0	0	0
Middleton									
Labradorite	53.6	-7.87	42.1	0.626	-10.91	45.2	0	0	0
Sanidine	5.5	-10.06	51.7	0.5	-12.41	38	-21.2	94.1	-0.823
Augite	17.2	-6.82	78	0.7	-11.97	78	0	0	0
Cordierite	1.3	-3.8	113.3	1	-11.2	28.3	0	0	0
Quartz	6.5	-	-	-	-13.99	87.7	-16.29	108366	-0.5
Ilmenite	2.4	-8.35	37.9	0.421	-11.16	37.9	0	0	0
Phlogopite	3.8				-12.4	29	0	0	0
Chlorite-smectite	8.6	-11.11	88	0.5	-12.52	88	0	0	0
Apatite	1.1	-3.73	250	0.613	-8	250	0	0	0
Hillhouse:									
Labradorite	34.6	-7.87	42.1	0.626	-10.91	45.2	0	0	0
Augite	32.7	-6.82	78	0.7	-11.97	78	0	0	0
Forsterite	14.7	-6.85	67.2	0.47	-10.64	79	0	0	0
Spinel	4.5	0	0	0	0	0	0	0	0
Ilmenite	0.6	-8.35	37.9	0.421	-11.16	37.9	0	0	0
Analcime	7.1	0	0	0	0	0	0	0	0
Biotite	0.4	-9.84	22	0.525	-12.55	22	0	0	0
Chlorite-smectite	5.2	-11.11	88	0.5	-12.52	88	0	0	0
Apatite	0.1	-3.73	250	0.613	-8	250	0	0	0

Table S4. Nitrogen cycle transformations: reactions and stoichiometry implemented in UK simulations.

Nitrogen fluxes and transformations	**Reaction or stoichiometry**
1. Ammonium (NH_4^+) gain, H^+ loss, OH^- gain	
Ammonification (mineralisation of organic N)	$NH_2\text{-}CO\text{-}NH_2 + 3H_2O \rightarrow \mathbf{2NH_4^+} + \mathbf{2OH^-} + CO_2$
Deposition from the atmosphere	One $\mathbf{H^+}$ **removed** per $\mathbf{NH_4^+}$ deposited
Ammonium fertilisers	One $\mathbf{H^+}$ **removed** per $\mathbf{NH_4^+}$ added
2. Ammonium (NH_4^+) loss, H^+ gain	
Nitrification	$\mathbf{NH_4^+} + 2O_2 \rightarrow \mathbf{NO_3^-} + H_2O + \mathbf{2H^+}$
NO emissions during nitrification	$\mathbf{NH_4^+} + 1.25O_2 \rightarrow \mathbf{NO} + 1.5H_2O + \mathbf{H^+}$
N_2O emissions during nitrification	$\mathbf{NH_4^+} + O_2 \rightarrow 0.5\ \mathbf{N_2O} + 1.5\ H_2O + \mathbf{H^+}$
Ammonia volatilisation	$\mathbf{NH_4^+} \leftrightarrows \mathbf{NH_3} + \mathbf{H^+}$
Uptake by plants and immobilisation by microbes	One $\mathbf{H^+}$ **added** per $\mathbf{NH_4^+}$ removed
3. Nitrate (NO_3^-) gain, H+ gain	
Nitrification	$\mathbf{NH_4^+} + 2O_2 \rightarrow \mathbf{NO_3^-} + H_2O + \mathbf{2H^+}$
Deposition from the atmosphere	One $\mathbf{H^+}$ **added** per $\mathbf{NO_3^-}$ added
Nitrate fertilisers	One $\mathbf{H^+}$ **added** per $\mathbf{NO_3^-}$ added
4. Nitrate loss (NO_3^-), H^+ loss	
N_2 gas emissions during denitrification	$\mathbf{NO_3^-} + 1.25CH_2O + \mathbf{H^+} \rightarrow 0.5\mathbf{N_2} + 1.25CO_2 + 1.75\ H_2O$
N_2O gas emissions during denitrification	$\mathbf{NO_3^-} + CH_2O + \mathbf{H^+} \rightarrow 0.5\mathbf{N_2O} + CO_2 + 1.5H_2O$
NO gas emissions during denitrification	$\mathbf{NO_3^-} + 1.75CH_2O + \mathbf{H^+} \rightarrow \mathbf{NO} + 0.75CO_2 + 1.25H_2O$
Uptake by plants and immobilisation by microbes	One $\mathbf{H^+}$ **removed** per $\mathbf{NO_3^-}$ removed

Table S5. Contribution of CLM5 N-cycle fluxes[16] to soil solution acidity.

Contribution of CLM5 nitrogen fluxes to soil acidity		
Flux (gN m^{-3}soil s^{-1}) in CLM5 (Eq. S1: $F_{i,N}$)	**$\Delta H_{i,N}$ mol H^+ mol^{-1} N**	**Flux description**
ACTUAL_IMMOB_NH4	+1	Immobilisation of ammonium by microbes
F_NIT	+2	Soil nitrification flux
F_N2O_NIT	+1	N_2O flux due to nitrification
F_NOx_NIT	+1	NO flux due to nitrification
SMINN_TO_PLANT_FUN_NH4	+1	Ammonium uptake by plants
F_NH3_VOL	+1	Ammonia volatilisation
GROSS_SMINN	–1	Soil organic matter N mineralisation to ammonium
SMINN_TO_PLANT_FUN_NO3	–1	Nitrate uptake by plants
ACTUAL_IMMOB_NO3	–1	Immobilisation of nitrate by microbes
F_N2O_DENIT	–1	N_2O flux due to denitrification
F_NOx_DENIT	–1	NO flux due to denitrification
F_N2_DENIT	–1	N_2 flux due to denitrification
NDEP_TO_SMINN	–1	N deposition from the atmosphere
FERT_TO_SMINN	–1	N fertiliser application
NFIX_TO_SMINN	–1	Symbiotic N fixation flux to soil ammonium
FFIX_TO_SMINN	–1	N fixation by free-living microbes to soil ammonium

Table S6. Observed, inventory and modelled UK arable N-gas emissions. Nitrogen fertilisers in CLM5 comprise manure and synthetic fertiliser applied as $NH4^+$. Values are average ± standard deviation for UK-NAEI, EMEP, CEDS, EDGAR and CLM5 (2010-2018) and average ± standard deviation of the mean for observations. Soil agriculture emissions for EMEP, EDGAR and CEDS were adjusted to account only for synthetic fertilizer and manure in arable land using fractions from UK-NAEI; observational fluxes in the UK were up-scaled to total arable land considering a 4.16 Mha UK crop area.

	N_2O (kt N yr^{-1})	**NO_x** (kt N yr^{-1})	**NH_3** (kt N yr^{-1})
CLM5-UK (this work)	8.6 ± 1.1	4.1 ± 0.5	63.7 ± 7.1
UK-NAEI[a]	5.0 ± 0.1	4.6 ± 0.1	73.5 ± 3.9
EMEP[b]	NA	4.9 ± 0.1	83.8 ± 4.1
EDGAR[c]	3.4 ± 0.1	5.4 ± 0.1	104.4 ± 5.6
CEDS-CMIP6[d]	5.2 ± 0.1	5.8 ± 0.2	128.2 ± 3.1
Observations[e]	12.5 ± 2.1	3.1 ± 0.9	48.3 ± 12.5

[a]UK National Atmospheric Emission Inventory (NAEI)[28]

[b]European Monitoring and Evaluation Programme (EMEP)[29]

[c]Emissions Database for Global Atmospheric Research (EDGAR)[30]

[d]Community Emissions Data System (CEDS)[31]

[e]Compilation of fluxes in UK croplands [32-37]. This broad observation-based estimate includes data gathered from field experiments with a wide range of fertilizer application rates (0-450 kg N/ha); higher fertilizer application rates drive the estimate upwards.

Table S7. Carbon emissions for fertilizers. Average values were obtained for P and K fertilizers across time horizons from the methodologies reported in the Ecoinvent LCIA database, which splits multi-products activities based on physical properties[38]. Global Markets for these products have been selected for this analysis to include all that those fertilisers coming to the UK from any region of the world. Therefore, all of the processes, including average transport distances, are considered. Values are converted to our emission's functional unit of CO_{2eq} per tonne.

LCIA	**Impact**	**Per tonne of potassium fertiliser, as K_2O**	**Per tonne of phosphate fertiliser, as P_2O_5**
ReCiPe Midpoint (H) V1.13	GWP100	0.349	1.737
TRACI	global warming	0.352	1.724
EDIP	global warming, GWP 100a	0.352	1.736
	global warming, GWP 20a	0.362	1.916
	global warming, GWP 500a	0.296	1.655
CML 2001	GWP 100a	0.353	1.742
	GWP 20a	0.370	1.961
	GWP 500a	0.294	1.654
	lower limit of net GWP	0.356	1.758
	upper limit of net GWP	0.361	1.764
IPCC 2013	GTP 100a	0.323	1.650
	GTP 20a	0.374	1.958
	GWP 100a	0.348	1.769
	GWP 20a	0.383	2.040

Supplementary references

1. Cameron, D.G. *et al. Directory of Mines and Quarries*. (British Geological Survey, Keyworth, UK, 2020).
2. Bide, T. *United Kingdom Minerals Yearbook* (British Geological Survey, Keyworth, UK 2010)
3. Mineral Products Association. *Long-term aggregates demand and supply scenarios, 2016-2030* (Mineral Products Association, London, 12 pp. 2017).
4. Lewis, A. L. *et al.* Effects of mineralogy, chemistry and physical properties of basalts on carbon capture potential and plant-nutrient element release via enhanced weathering. *App. Geochem.* **132,** 105023 (2021).
5. Emmett, B.A. *et al. Countryside Survey: Soils Report from 2007* (Technical Report No. 9/07, NERC/Centre for Ecology & Hydrology, 2010).
6. Fischer, G. *et al.* Global agro-ecological zones assessment for agriculture. (IIASA, Laxenburg, Austria and FAO, Rome, Italy 2008).
7. Goulding, K.W.T. Soil acidification and the importance of liming, agricultural soils with particular reference to the United Kingdom. *Soil Use Manag.* **32,** 390-399 (2016).
8. McNally, A. FLDAS Noah Land Surface Model L4 Global Monthly 0.1 × 0.1 degree (MERRA-2 and CHIRPS). (GES DISC, Greenbelt, MD, USA, 2018).
9. UKCEH. Land Cover® plus: Crops. (UKCEH, Bangor, UK, 2019).
10. Monfreda, C., Ramankutty, N. & Foley, J.A., Farming the planet: 2. Geographic distribution of crop areas, yields, physiological types, and net primary production in the year 2000. *Global Biogeochem Cycles* **22,** GB1022 (2008).
11. Breiman, L. *Classification and regression trees* (Wadsworth International Group, Belmont, Calif., 358 pp. 1984).
12. Renforth, P. & Henderson, G. Assessing ocean alkalinity for carbon sequestration. *Rev. Geophy.* **55**, 636–674 (2017).
13. Beerling, D. J. *et al.* Potential for large-scale CO_2 removal via enhanced rock weathering with croplands. *Nature* **583**, 242–248 (2020).
14. Brantley, S. L. in *Kinetics of water-rock interaction* (eds Susan L Brantley, James D Kubicki, & Art F White) Ch. 5, 151–210 (Springer, 2008).
15. Palandri, J. L. & Kharaka, Y. K. A compilation of rate parameters of water-mineral interaction kinetics for application to geochemical modeling. *Open File Report 2004-1068*, 64 pages (2004).
16. Lawrence, D. *et al.* Technical description of version 5.0 of the Community Land Model (CLM). 329 pages (Boulder, CO, 2018).
17. Bolan, N. S. & Hedley, M. J. in *Handbook of soil acidity* (ed Zdenko Rengel) Ch. 2, 29–56 (Marcel Dekker, Inc., 2003).
18. Fageria, N. K., Baligar, V. C. & Jones, C. A. *Growth and mineral nutrition of field crops*. 3rd edn, (CRC Press, 2010).
19. Brzostek, E. R., Fisher, J. B. & Phillips, R. P. Modeling the carbon cost of plant nitrogen acquisition: Mycorrhizal trade-offs and multipath resistance uptake improve predictions of retranslocation. *J. Geophys. Res.: Biogeosci.* **119**, 1684–1697 (2014).
20. Berner, R. A. Rate control of mineral dissolution under earth surface conditions. *Am. J. Sci.* **278**, 1235–1252, doi:10.2475/ajs.278.9.123 (1978).
21. Maher, K. The dependence of chemical weathering rates on fluid residence time. *Earth Plan. Sci. Lett.* **294**, 101–110, doi:10.1016/j.epsl.2010.03.010 (2010).
22. Dessert, C., Dupré, B., Gaillardet, J., François, L. M. & Allegre, C. J. Basalt weathering laws and the impact of basalt weathering on the global carbon cycle. *Chem. Geol.* **202**, 257–273 (2003).
23. Mercure, J. F. *et al.* Macroeconomic impact of stranded fossil fuel assets. *Nat. Clim. Change* **8**, 588–593 (2018).
24. Mercure, J.-F. *et al.* Environmental impact assessment for climate change policy with the simulation-based integrated assessment model E3ME-FTT-GENIE. *Energy Strat. Rev.* **20**, 195–208 (2018).
25. Cambridge Econometrics. *E3ME Manual: Version 6.1*, <http://www.e3me.com> (2019).
26. Holden, P. B. *et al.* Climate–carbon cycle uncertainties and the Paris Agreement. *Nat. Clim. Change* **8**, 609–613 (2018).

27. HM Government. *The Energy White Paper. Powering our Net Zero Future*. (Queen's Printer and Controller of Her Majesty's Stationery Office, 2020).
28. Department for Business Energy and Industrial Strategy. *UK National Atmospheric Emissions Inventory*, <https://naei.beis.gov.uk/data/> (2021).
29. European Monitoring and Evaluation Programme. *EMEP Centre on Emission Inventories and Projections*, < https://www.ceip.at/webdab-emission-database/reported-emissiondata> (2021).
30. Crippa, M. *et al.* High resolution temporal profiles in the Emissions Database for Global Atmospheric Research. *Sci. Data* **7**, 1–17 (2020).
31. Hoesly, R. M. *et al.* Historical (1750–2014) anthropogenic emissions of reactive gases and aerosols from the Community Emissions Data System (CEDS). *Geo. Mod. Dev.* **11**, 369–408 (2018).
32. Kim, D.-G., Saggar, S. & Roudier, P. The effect of nitrification inhibitors on soil ammonia emissions in nitrogen managed soils: a meta-analysis. *J. Nutr. Cyc. Agro.* **93**, 51–64 (2012).
33. Fitton, N. *et al.* Assessing the sensitivity of modelled estimates of N_2O emissions and yield to input uncertainty at a UK cropland experimental site using the DailyDayCent model. *J. Nutr. Cyc. Agro.* **99**, 119–133 (2014).
34. Bell, M. *et al.* Nitrous oxide emissions from fertilised UK arable soils: fluxes, emission factors and mitigation. *Agri. Eco. Environ.* **212**, 134–147 (2015).
35. Liu, S. *et al.* A meta-analysis of fertilizer-induced soil NO and combined NO+N_2O emissions. *Global Change Biology* **23**, 2520–2532 (2017).
36. Wang, Y. *et al.* Soil pH as the chief modifier for regional nitrous oxide emissions: new evidence and implications for global estimates and mitigation. *Glob. Change Biol.* **24**, e617–e626 (2018).
37. Huddell, A. M. *et al.* Meta-analysis on the potential for increasing nitrogen losses from intensifying tropical agriculture. *Glob. Change Biol.* **26**, 1668–1680, (2020).
38. Wernet, G. *et al.* The ecoinvent database version 3 (part I): overview and methodology. *Int. J. Life Cycle Assess.* **21**, 1218-1230 (2016).